IEEE Access
Multidisciplinary | Rapid Review | Open Access Journal

Received September 10, 2019, accepted September 25, 2019, date of publication October 1, 2019, date of current version October 15, 2019.

Digital Object Identifier 10.1109/ACCESS.2019.2944964

An Improved Particle Swarm Optimization Algorithm Suitable for Photovoltaic Power Tracking Under Partial Shading Conditions

KEYONG HU[1,2], (Member, IEEE), SHIHUA CAO[1], (Member, IEEE), WENJUAN LI[1], (Member, IEEE), AND FANGMING ZHU[3], (Member, IEEE)

[1]Qianjiang College, Hangzhou Normal University, Hangzhou 310018, China
[2]College of Mechanical Engineering, Zhejiang University of Technology, Hangzhou 310014, China
[3]School of Information Science and Engineering, Hangzhou Normal University, Hangzhou 311121, China

Corresponding author: Keyong Hu (hukeyong@yeah.net)

This work was supported in part by the Natural Science Foundation of Zhejiang Province in China under Grant LY17E070004 and Grant LY17F010010, in part by the First Group of Teaching Reform Research Projects in the 13th Five-Year Plan of Higher Education in Zhejiang Province under Grant jg20180509, in part by the Research Project of Educational Science Planning in Zhejiang of China under Grant 2018SCG015, in part by the Research Projects of Laboratory Work in Universities and Colleges of Zhejiang Province under Grant YB201904, in part by the Academic Scientific Research Funding Project under Grant 2019QJJL05, and in part by the Natural Science Foundation of China under Grant 61702151.

ABSTRACT The partial shading of a photovoltaic array repeatedly occurs in the natural environment, which can cause a failure of a conventional maximum power point tracking (MPPT) algorithm. In this paper, the convergence conditions of the standard particle swarm optimization (PSO) algorithm are deduced by the functional analysis, and then the influence of the random variables and inertia factor of the algorithm on the trajectory in the particle swarm optimization is analyzed. Based on the analysis results, an improved particle swarm optimization (IPSO) algorithm, which adopts both global and local modes to locate the maximum power point, is proposed. Compared to the standard PSO algorithm, in the improved PSO algorithm, many random and interfered variables are removed, and the structure is optimized significantly. The proposed algorithm is first simulated in MATLAB to ensure its capability. The feasibility of the approach is validated through physical implementation and experimentation. Results demonstrate that the proposed algorithm has the capability to track the global maximum power point within 3.3 s with an accuracy of 99%. Compared with five recently developed Global MPPT algorithms, the proposed IPSO algorithm achieved better performance in the maximum power tracking in the partial shading conditions.

INDEX TERMS Maximum power point tracking, partial shade, particle swarm optimization, photovoltaic array.

I. INTRODUCTION

The power–voltage ($P - V$) characteristic of a photovoltaic (PV) module shows its operating point, which denotes the point at which module can output the maximum power, and it is known as the maximum power point (MPP). The position of the MPP depends on the external environment, and it changes with the change in the environmental conditions. Therefore, the maximum-power-point tracking (MPPT) methods for a PV system are required to maintain efficient power output. Recently, several MPPT methods have been proposed. However, the Perturb and Observation (P&O) [1]–[4] and the Incremental Conductance (IncCond) [5]–[8] are the most commonly used methods. Although these methods are easy to implement, they are unable to track the MPP accurately under the partial shading conditions (PSC) due to the inability to distinguish between a local MPP and the global peak (GP) [9]–[12]. Therefore, some studies have proposed a new modified P&O (MPPT) method with adaptive duty cycle step size using fuzzy logic controller [13]. A new incremental conductance controller is developed, based on a fuzzy duty cycle change estimator with direct control [14].

In the related literature, there are many MPPT methods [15]–[19]. These methods can be classified into two main categories: indirect methods and direct methods. The indirect

The associate editor coordinating the review of this manuscript and approving it for publication was Sotirios Goudos.

methods establish the mathematics model using the physical parameters of a solar cell, and when the external variables are fed to the model input, the maximum power point of a PV system can be quickly estimated [15]–[17]. On the other hand, the direct methods use the on-line measured voltage and current of a PV system and obtain the maximum power point by using the tracker. These methods are less dependent on the physical parameters of a solar cell, but the tracking precision of the maximum power point is low [18], [19].

In [20], a direct method was adopted, and a simulated annealing (SA)-based global maximum power point tracking (GMPPT) technique designed for PV systems that experience partial shading conditions was proposed; also, it was found that a conventional MPPT algorithm under the partial shading conditions could not track the maximum power point effectively. In most MPPT algorithms it is considered that there is only one, a single peak in the *P–V* characteristic of a PV module [21]. However, when a PSC occurs, the *P–V* characteristic exhibits multiple peaks, so the traditional MPPT algorithms cannot determine which of the peaks denotes the maximum power point, which reduces the entire output power of a PV system [22]–[25]. Recently, to improve the MPP tracking accuracy and system dynamic response, several modified MPPT methods have been proposed [26]–[29]. In [30], an improved global search space differential evolution (DE) algorithm for tracking the GMPP is introduced, optimization algorithm can search for the GMPP within a larger operating region and quickly response against load variation. In [31], the relationship between the load line and the *I-V* curve is used with trigonometry rule to obtain the fast response. In [32], it reviews AI-based techniques proven to be effective and feasible to implement for MPPT, including their limitations and advantages.

In recent years, another technology has been proposed for the MPPT, named the particle swarm optimization (PSO) technique [33]–[36]. The PSO technique has the advantages of easy implementation, fast computation, and strong environmental adaptability [37], [38]. Moreover, it can perform a more flexible search than other evolutionary techniques, such as the Genetic Algorithm (GA) [39]. Also, the duty cycle based on the particle velocity is variable, while the duty cycle of the other techniques is easy to perturb by a fixed value. Therefore, by approaching the maximum power point, the searching oscillations tend to be stable. However, the PSO algorithm has a few shortcomings. Since the particles in the standard PSO are randomly initialized in the searching space, the convergence time of approaching the maximum power point is longer, which results in a large-amount computation. Meanwhile, although a proper initialization of the particles can improve the efficiency of the PSO algorithm and lead to the faster convergence, the initialization process of the swarm in the PSO is not easy to control. The conventional MPPT algorithm combined with the PSO and a two-stage algorithm was proposed in [26]. In the first stage, the nearest local maximum was detected by the conventional MPPT method, and in the second stage, the obtained information was used for tracking the GP by the PSO algorithm; however, this method was not efficient in more complex shading conditions.

Another advantage of the PSO algorithm is that it treats the maximum power tracking problem as an optimization problem. Due to the ability of the PSO to handle multi-modal objective functions, in [40]–[42], the PSO was applied to search the GP in the partial shading conditions. However, the random variables of the PSO algorithm can reduce the searching efficiency significantly in the optimization process, so more searching iterations need to be executed. On the other hand, since the PSO algorithm contains the random variables, the operation process of the algorithm is complex, which not only makes the control difficult but also can easily cause falling into a local optimum. In addition, the perturbation in the PSO is related to the number of iterations of the algorithm itself. When the random values are too small, the time for reaching the algorithm reference value extends, and the number of iterations increases; when the random values are too large, the searching particles may omit the maximum power point and fall into a local optimum. Therefore, it is necessary to study the convergence constraints of the PSO algorithm and the effect of its random variables on the particle trajectory. However, the research on this subject has been rarely conducted in recent studies.

Considering the mentioned PSO drawbacks, this paper proposes an improved method to augment the MPPT method for a PV system under partial shading. The novel of this paper is listed as follows:

(1) By functional analysis, the convergence conditions of standard PSO algorithm are derived.

(2) Through comparative analysis of parameters, the influence of random variables and inertia factors in the PSO algorithm on the convergence is obtained.

(3) An improved particle swarm optimization (IPSO) algorithm, which adopts both global and local modes to locate the maximum power point, is proposed. The proposed algorithm is particularly suitable for tracking global power point under local shading.

The paper is organized as follows. In Section I, the research on the MPPT when PV modules are under the partial shading is presented, and the advantages and disadvantages of the PSO used are discussed. In Section II, first the characteristics of photovoltaic cells are presented, the equivalent circuit model is given, and the reasons for multiple peaks in the *P-V* characteristic when PV modules are sheltered from a local shadow are analyzed. In Section III, the standard particle swarm optimization algorithm is analyzed, and the constraint conditions of the particle swarm convergence are deduced by the functional analysis. In Section IV, the influence of the random variables and inertia factor of the algorithm on a trajectory in the particle swarm optimization is explored, and the conception of an improved particle swarm optimization algorithm is presented. In Section V, an improved method to augment the MPPT method for the PV system under the partial shading conditions is described. In Section VI, first the simulation platform of the MPPT is introduced, then the

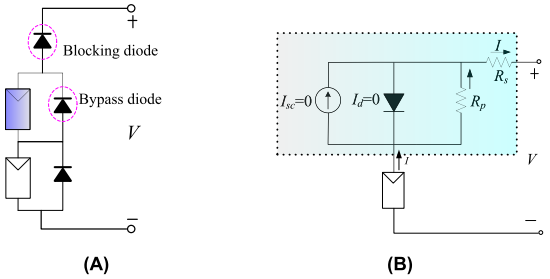

FIGURE 1. The equivalent model of a PV array under the partial shading conditions; (A) Physical model of a PV array; (B) Circuit model of a PV array.

standard and improved PSO algorithms are respectively applied to the simulation platform, and lastly, the simulation results are compared and analyzed. In Section VII, the experimental platform is described, and the MPPT experiment of a PV module under shading conditions is carried out using the PSO, an improved particle swarm optimization (IPSO), and fuzzy logic control (FLC) algorithms, and then, the experimental results are compared. Lastly, a brief conclusion is given in Section VIII.

II. P-V CHARACTERISTIC UNDER PARTIAL CONDITION

The equivalent model of a PV array under the partial shading conditions is presented in Fig. 1. Since the PV modules are connected in series, in the case of partial shading, the current flowing through all the PV modules is the same. When one of the PV modules is shaded (for instance, the first PV module), the photocurrent I_{sc} drops rapidly to zero. Namely, the shaded diode has a reverse bias, so the bias current I_d reduces to zero; thus, the current I causes a voltage drop (V_c) through R_p and R_s which can be expressed by:

$$V_c = -(R_p + R_s)I \tag{1}$$

where R_p is the equivalent parallel resistance of a photovoltaic module, R_s is the equivalent serial resistance of a photovoltaic module, and I is the output current of a photovoltaic module. As voltage drop V_c has a negative value, it needs to be removed from the final output voltage, which forms a hot spot on the shaded position. The appearance of the hot spot not only reduces the output power but also shortens the service life of PV modules. A better way to protect the PV modules is to use the bypass diodes, which can make the excess current bypass the shaded module.

In order to simplify the analysis of the electrical characteristics of shading, a PV array composed of two PV modules connected in series is used. Assume that one PV module is fully sun-lighted, and the other one is shaded. In this case, since the modules are connected in series, the current flowing through the two PV modules is the same. The current generated by the shaded module is less than that of the sun-lighted (unshaded) module, so that the excess current will pass through the bypass diode. The corresponding I-V characteristic is shown in Fig. 2.

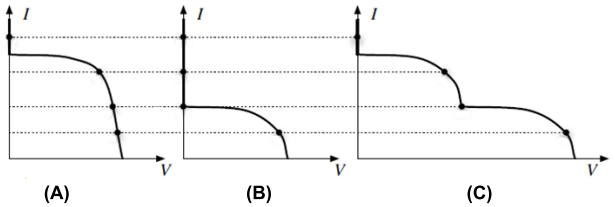

FIGURE 2. The multi-peak I-V characteristic of the PV array; (A) Not shading module; (B) Shading module; (C) Series of a PV array.

In Fig. 2, the photovoltaic modules are connected in series. Thus, when the modules receive a different level of sunlight, the output voltage has multiple peaks, which further results in many peaks in the final output power. With the increase in the number of photovoltaic modules, the I-V characteristic of PV modules becomes more complex, containing more peaks. Thus, it is difficult to track the maximum power point by the conventional methods.

III. ANALYSIS OF PSO ALGORITHM

A. STANDARD PSO

The mathematical description of the PSO algorithm is as follows. Assume the i^{th} particle contains an N-dimensional position vector defined as $\boldsymbol{x_i} = (\boldsymbol{x_{i1}}, \boldsymbol{x_{i2}}, \ldots, \boldsymbol{x_{iN}})$, and a velocity vector defined as $\boldsymbol{v_i} = (\boldsymbol{v_{i1}}, \boldsymbol{v_{i2}}, \ldots, \boldsymbol{v_{iN}})$. When the i^{th} particle searches in the solution space, it will remember the optimal experience location $\boldsymbol{p_i} = (\boldsymbol{p_{i1}}, \boldsymbol{p_{i2}}, \ldots, \boldsymbol{p_{iN}})$. At the beginning of every iteration, the particles adjust their speed vectors according to their inertia and optimal experience location of group $\boldsymbol{p_g} = (\boldsymbol{p_{g1}}, \boldsymbol{p_{g2}}, \ldots, \boldsymbol{p_{gN}})$, so as to adjust their positions. The acceleration factors c_1 and c_2 and the random variables r_1 and r_2 are all in the range [0, 1]. Also, $\boldsymbol{v_i} \in [-v_{\max}, v_{\max}]$, where $v_{\max}$ denotes a speed factor, and it is set by a user, and w denotes an inertia weight factor. The position and speed of a particle are updated by the following formulas:

$$v_i^{k+1} = wv_i^k + c_1 r_1 (p_i - x_i^k) + c_2 r_2 (p_g - x_i^k) \tag{2}$$

$$x_i^{k+1} = x_i^k + v_i^{k+1} \tag{3}$$

where x_i^k is the position of the i^{th} particle in the k^{th} generation, v_i^k is the speed of the i^{th} particle in the k^{th} generation, x_i^{k+1} is the position of the i^{th} particle in the $(k+1)^{\text{th}}$ generation, v_i^{k+1} is the speed of the i^{th} particle in the $(k+1)^{\text{th}}$ generation, $\mathrm{p_i}$ is the optimal experience position of the i^{th} particle, and lastly, $\boldsymbol{p_g}$ is the optimal experience position of the group. The particle position updating process in a generation is shown in Fig. 3.

Since the particle swarm optimization algorithm adopts the searching technology based on the neighborhood principle, it can use a small number of particles to ensure enough diversity and search for an optimal solution simultaneously. Meanwhile, the particle swarm optimization has good universality, which is suitable for dealing with various kinds of objective functions and constraints and can be easily combined with

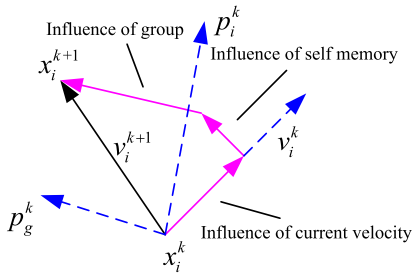

FIGURE 3. The particle position updating process.

the traditional optimization methods, so as to avoid its limitations. Therefore, in this study, the PSO algorithm is improved and applied to the photovoltaic maximum power tracking in the shading conditions.

B. CONVERGENCE ANALYSIS OF PSO ALGORITHM

In order to optimize the power of photovoltaic arrays by the PSO algorithm, the primary premise is to ensure that the position and speed of a searching particle are convergent. Considering the relationship between p_i and various dimensions of a searching space, the update of each dimension is independent; thus, the algorithm analysis can be simplified to one dimension. Assume that only the i^{th} particle is moving and the other particles in this group are stationary. Then, when the behavior of a single particle is analyzed, (2) and (3) are respectively equivalent to the following formulas:

$$v^{k+1} = wv^k + \varphi_1(p - x^k) + \varphi_2(p_g - x^k) \tag{4}$$

$$x^{k+1} = x^k + v^{k+1} \tag{5}$$

where $\varphi_1 = c_1 r_1$, $\varphi_2 = c_2 r_2$.

Because all φ_1 , φ_2 , w are constant, when k changes, p and p_g remain unchanged. By combining (4) and (5), we get:

$$x^{k+1} = (1 + w - \varphi)x^k - wx^{k-1} + \varphi_1 p + \varphi_2 p_g \tag{6}$$

where $\varphi = \varphi_1 + \varphi_2$.

In order to deduce the convergence condition, the position vector defined by (6) is expressed as follow:

$$x^k = a + b\beta^k + c\gamma^k \tag{7}$$

where:

$$\begin{aligned}
a &= \frac{\varphi_1 p + \varphi_2 p_g}{\varphi} \\
b &= \frac{\gamma(x_0 - x_1) + (w - \varphi)x_1 - wx_0 + \varphi_1 p + \varphi_2 p_g}{(\beta - 1)\sqrt{(1 + w - \varphi)^2 - 4w}} \\
c &= \frac{\beta(x_0 - x_1) + (w - \varphi)x_1 + wx_0 - \varphi_1 p - \varphi_2 p_g}{(\gamma - 1)\sqrt{(1 + w - \varphi)^2 - 4w}} \\
\beta &= \frac{1 + w - \varphi + \sqrt{(1 + w - \varphi)^2 - 4w}}{2} \\
\gamma &= \frac{1 + w - \varphi - \sqrt{(1 + w - \varphi)^2 - 4w}}{2}
\end{aligned} \tag{8}$$

x_0 and x_1 are two initial values of (7).

The convergence of (7) depends on the values of β and γ. Based on the mathematical theory of limit, three cases are possible, and they are listed in the following.

(1) In the first case, it holds that:

$$(1 + w - \varphi)^2 - 4w < 0 \tag{9}$$

where β and γ are the complex numbers that are determined by the two-dimensional norm, that is, $\|\beta\| = \|\gamma\| = \sqrt{w}$. Following the principles of the applied functional mathematics, if $\max(\|\beta\|, \|\gamma\|) < 1$, that is, $0 < w < 1$, $\lim_{k\to\infty} x(k) = a$, then, the particle swarm is converged.

(2) In the second case, it holds that:

$$(1 + w - \varphi)^2 - 4w = 0 \tag{10}$$

Thus, it can be deduced that:

$$\|\beta\| = \|\gamma\| = \frac{|1 + w - \varphi|}{2} \tag{11}$$

If $\max(\|\beta\|, \|\gamma\|) < 1$, that is, $0 \le w \le 1$, $\lim_{k\to\infty} x(k) = a$, then the particle swarm is converged.

(3) In the third case, it holds that:

$$(1 + w - \varphi)^2 - 4w > 0 \tag{12}$$

This case can be divided into three sub-cases as follows.

(3.1) If $w > \varphi - 1$, and when $\max(\|\beta\|, \|\gamma\|) < 1$, due to $\|\beta\| > \|\gamma\|$, then $\|\beta\| < 1$, that is, $\|\beta\| = \frac{1+w-\varphi+\sqrt{(1+w-\varphi)^2-4w}}{2} < 1$, which is expressed by:

$$\sqrt{(1 + w - \varphi)^2 - 4w} < 1 - w + \varphi \tag{13}$$

By solving (13), $\varphi > 0$ and $w < 1 + \varphi$ can be obtained, so the convergence region of a particle swarm is defined by $\varphi > 0$, $\varphi - 1 < w < \varphi + 1$.

(3.2) If $w = \varphi - 1$, it holds that:

$$\|\beta\| = \|\gamma\| = \sqrt{-w} \tag{14}$$

If $\max(\|\beta\|, \|\gamma\|) < 1$, then $\sqrt{-w} < 1$, and as a result, $-1 < w < 0$ is obtained.

(3.3) If $w < \varphi - 1$ and $\max(\|\beta\|, \|\gamma\|) < 1$, since $\|\beta\| < \|\gamma\|$, then $\|\gamma\| < 1$, that is, $\|\gamma\| = \frac{-1-w+\varphi+\sqrt{(1+w-\varphi)^2-4w}}{2} < 1$, which is expressed by:

$$\sqrt{(1 + w - \varphi)^2 - 4w} < 3 + w - \varphi. \tag{15}$$

By solving (15), the convergence region of the particle swarm is defined by: $2w + 2 - \varphi > 0$ and $w < 1$.

Based on the above three cases, the convergence region of a particle swarm is an enclosed region defined by $(1 + w - \varphi)^2 - 4w > 0$, $2w + 2 - \varphi > 0$, $w < 1$, $\varphi > 0$, and it is shown in Fig. 4. Thus, the convergence conditions of the PSO algorithm are expressed as: $2w + 2 - \varphi > 0$, $0 < w < 1$ and $\varphi > 0$. The values of w, φ in this region satisfy the convergence of searching particles at each initial position and each initial velocity.

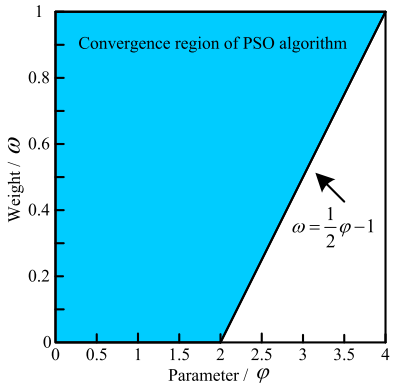

FIGURE 4. The convergence region of the PSO algorithm.

IV. EFFECT OF RANDOM VARIABLES ON PARTICLE TRAJECTORY

In the maximum power point tracking process of a PV array, the role of random variables in the particle swarm optimization is very important. Although the uncertainty of the random variables may bring diversity to the particle swarm, it can also add some unstable factors to the power optimization of a PV array. In order to analyze the effect of random variables on the maximum power point tracking performed by the PSO algorithm, it is necessary to study the effect of random variables on the particle trajectory. To facilitate the analysis, the solution space is simplified to one dimension. Assuming that p_i and p_g are constant, the state equations of the i^{th} particle can be expressed by:

$$\begin{aligned} v_i(t+1) &= wv_i(t) + c_1r_1[p_i - x_i(t)] + c_2r_2[p_g - x_i(t)] \\ &= wv_i(t) + \varphi_1[p_i - x_i(t)] + \varphi_2[p_g - x_i(t)] \quad (16) \\ x_i(t+1) &= x_i(t) + v_i(t+1) \quad (17) \end{aligned}$$

where $\varphi_1 = c_1r_1$ and $\varphi_2 = c_2r_2$.

In (16), the discrete time point is moved back by one step, and when (17) is substituted into (16), we get:

$$v_i(t+2) = wv_i(t+1) - (\varphi_1 + \varphi_2)[x_i(t) + v_i(t+1)] + \varphi_1p_i + \varphi_2p_g \quad (18)$$

where $-(\varphi_1 + \varphi_2)x_i(t) = v_i(t+1) - wv_i(t) - \varphi_1p_i - \varphi_2p_g$ is deduced from (16), and then substituted into (18), which leads to the following formula:

$$v_i(t+2) + (\varphi_1 + \varphi_2 - w - 1)v_i(t+1) + wv_i(t) = 0 \quad (19)$$

As can be seen in (19), the velocity change of the i^{th} particle conforms to the second-order derivative equation. When p_i and p_g are assumed to remain unchanged during the movement, the velocity change is independent of p_i and p_g.

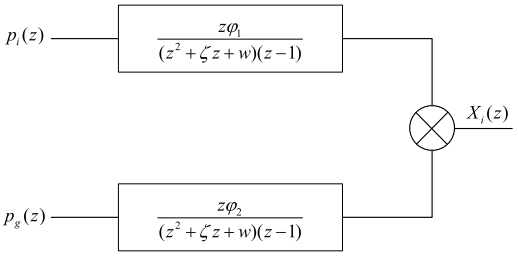

FIGURE 5. The effect of random variables on the particles' positions.

By using the same method, the position equation of the i^{th} particle can be deduced. By substituting (16) into (17), we get:

$$x_i(t+1) = x_i(t) + wv_i(t) + \varphi_1[p_i - x_i(t)] + \varphi_2[p_g - x_i(t)] \quad (20)$$

where $v_i(t) = x_i(t) - x_i(t-1)$, which is obtained by (17) and then substituted into (20). When the discrete time point is moved back by one step, we get:

$$x_i(t+2) = (1 + w - \varphi_1 - \varphi_2)x_i(t+1) - wx_i(t) + \varphi_1p_i + \varphi_2p_g \quad (21)$$

In (21), it can be seen that the trajectory of the i^{th} particle satisfies the second-order derivative equation.

The derivative equation (21) can be converted by the Z-transformation [43], which can be expressed as (22), as shown at the bottom of this page: where $\zeta = \varphi_1 + \varphi_2 - 1 - w$.

If the initial values of (22) are set to $x_i(0) = x_i(1) = 0$, then $p_i(t)$ and $p_g(t)$ can also be converted by the Z-transformation, which can be expressed by:

$$X_i(z) = \frac{z\varphi_1p_i(z) + z\varphi_2p_g(z)}{(z^2 + \zeta z + w)(z-1)} \quad (23)$$

(23) demonstrates the effect of the random variables on the particles' positions, which is also shown in Fig. 5. The random variables exist in $\varphi_1 = c_1r_1$, $\varphi_2 = c_2r_2$; therefore, the random variables in the control system cannot be treated as an interfering signal or a noise. The existence of random variables makes the whole control process be a complex nonlinear process, which can difficultly converge by applying conventional methods.

In order to clarify the influence of random variables on particle trajectory, five combinations of parameters are set up; thus, the optimal trajectories of particles may be intuitively detected.

(1) Combination of parameters #1: when $w = 0.7$, $\varphi_1 = 1.2$, and $\varphi_2 = 1.2$, the parameters meet the convergence conditions. The initial state is set to: $p_i = 5, p_g = 9, x(0) = 1$, and $v(0) = 2$. The evolution trajectory and velocity of the

$$X_i(z) = \frac{z^3x_i(0) + z^2[x_i(1) + (\zeta - 1)x_i(0)] + z[\varphi_1p_i + \varphi_2p_g - \zeta x_i(0) - x_i(1)]}{(z^2 + \zeta z + w)(z-1)} \quad (22)$$

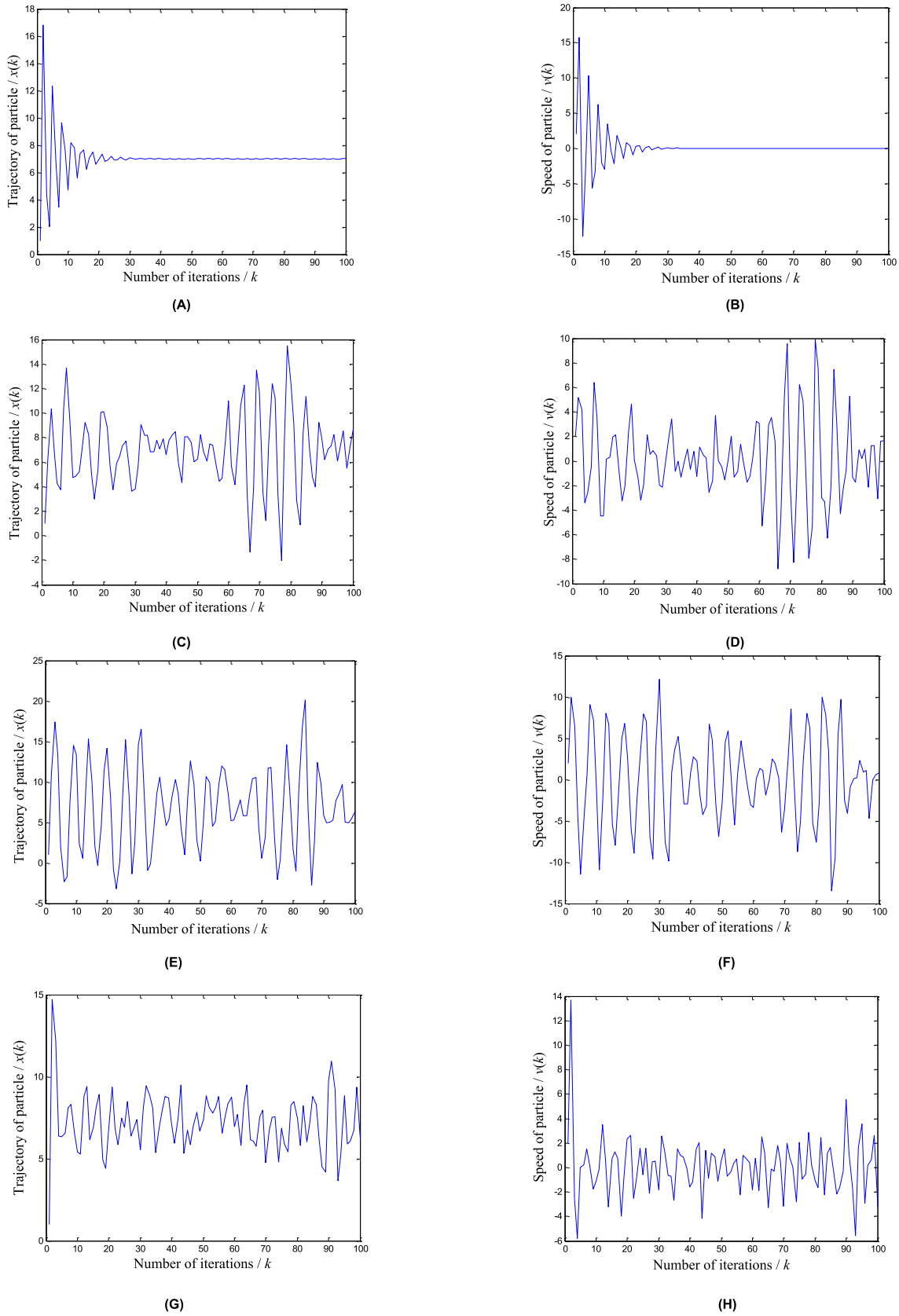

FIGURE 6. The particle motion process for five combinations of parameters; (A) The particle trajectory for combination #1; (B) The particle speed for combination #2; (C) The particle trajectory for combination #2; (D) The particle speed for combination #2; (E) The particle trajectory for combination #3; (F) The particle speed for combination #3; (G) The particle trajectory for combination #4; (H) The particle speed for combination #4; (I) The particle trajectory for combination #5; (J) The particle speed for combination #5.

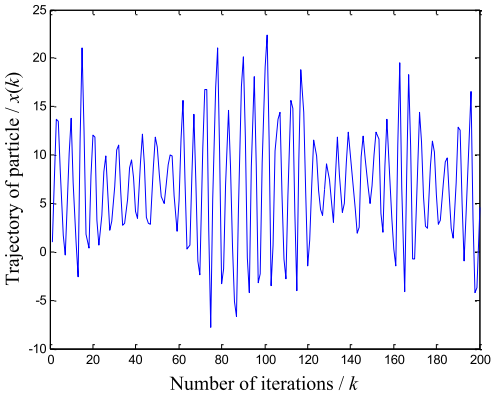

(I)

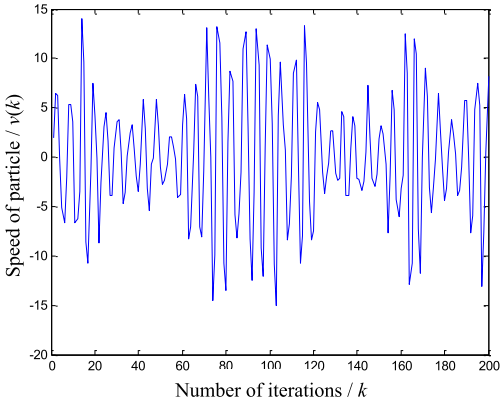

(J)

FIGURE 6. ***(Continued.)*** **The particle motion process for five combinations of parameters; (A) The particle trajectory for combination #1; (B) The particle speed for combination #2; (C) The particle trajectory for combination #2; (D) The particle speed for combination #2; (E) The particle trajectory for combination #3; (F) The particle speed for combination #3; (G) The particle trajectory for combination #4; (H) The particle speed for combination #4; (I) The particle trajectory for combination #5; (J) The particle speed for combination #5.**

particle are shown in Figs. 6 (A), (B). The particle movement belongs to the damping oscillation, its final trajectory converges to 7, and its final convergence speed is equal to 0.

(2) Combination of parameters #2: when $w = 0.7$, $\varphi_1 = 1.2^*rand(1)$, and $\varphi_2 = 1.2^*rand(1)$, the parameters meet the convergence conditions. The initial state is set to: $p_i = 5$, $p_g = 9$, $x(0) = 1$, and $v(0) = 2$. The evolution trajectory and velocity of the particle are shown in Figs. 6 (C), (D). The particle is always in the process of repeated movement, unable to converge to a fixed position.

(3) Combination of parameters #3: when $w = 0.9$, $\varphi_1 = 1.2^*rand(1)$, and $\varphi_2 = 1.2^*rand(1)$, the parameters meet the convergence conditions. The initial state is set to: $p_i = 5$, $p_g = 9$, $x(0) = 1$, and $v(0) = 2$. The evolution trajectory and velocity of the particle are shown in Figs. 6 (E), (F). The particle is always in the process of movement, and cannot converge to a fixed position. The oscillation amplitude of the particle is obviously greater than that at $w = 0.7$.

(4) Combination of parameters #4: when $w = 0.4$, $\varphi_1 = 1.2^*rand(1)$, and $\varphi_2 = 1.2^*rand(1)$, the parameters meet the convergence conditions. The initial state is set to: $p_i = 5$, $p_g = 9$, $x(0) = 1$, and $v(0) = 2$. The evolution trajectory and velocity of the particle are shown in Figs. 6 (G), (H). The oscillation amplitude of the particle is much smaller than that at $w = 0.7$; thus, the particle movement tends to be stable.

(5) Combination of parameters #5: when $w = 0.9$, $\varphi_1 = 1^*rand(1)$, and $\varphi_2 = 1^*rand(1)$, the parameters meet the convergence conditions. The initial state is set to:$p_i = 5$, $p_g = 9$, $x(0) = 1$, and $v(0) = 2$. The evolution trajectory and velocity of the particle are shown in Figs. 6 (I), (J). The particle quickly approaches the best position, but it cannot converge to the best position; namely, it immediately diverges, and then circulates.

Accordingly, it can be found that when the combination of parameters meets the convergence conditions of the PSO algorithm, the particle motion is not necessarily stable, so it is difficult to ensure that the particle finds the maximum power point. Apparently, due to the existence of random variables, the particle trajectory is not always in accordance with the convergence law; in other words, the traditional particle swarm algorithm may cause the PV optimization to fall into the local optimum, missing to locate the real maximum power point.

The results of different parameter combinations also show that when a combination of parameters is close to the convergent boundary, the probability that the particle is stabilized to a fixed position is reduced, and vice versa. Therefore, the influence of the inertial factor w is very large. The larger the inertial factor w is, the higher the probability of non-convergence is, and vice versa. Moreover, the oscillation amplitude is closely related to the choice of parameters. Namely, when the combination of parameters does not meet the convergence conditions, the oscillatory fluctuation is more intense, and sometimes even the oscillation tends to diverge. On the other hand, when a combination of parameters meets the convergence conditions, the oscillation amplitude is greatly influenced by the inertia factor w. The larger the inertial factor w is, the larger the oscillation amplitude is. This helps to expand the range of particle optimization and accelerate the searching speed of a particle.

According to the analysis given in the previous section, when the traditional particle swarm algorithm is applied to the power optimization control of a PV array, some uncontrollable factors will be faced. As can be seen in (16) and (17), the update of a particle position is related to the change in the random variables, so there are two uncontrollable factors.

(1) When the change in the random variables' values is larger, the particle velocity variation is also larger. The particle can very easy omit to find the global peak and go to the surrounding area of a local peak. As a result, the particle swarm optimization finds a local optimum instead of the global optimum. At present, if the standard particle swarm

optimization algorithm is applied to the MPPT of a PV array, the difference between a local peak and the global peak cannot be directly differentiated.

(2) When the change in the random variables' values is smaller, the particle velocity variation is also smaller; so it takes a longer time to a particle to arrive at a new position, and a large number of iterations are needed to approach the target position. As a result, real-time performance is poor, and a large amount of calculation is caused.

By considering the above two problems, the standard PSO algorithm is improved in this work. To reduce the influence of random variables, first, the convergence direction of velocity has to be consistent, and then the maximum power point can be searched by a small-step perturbation. To achieve this goal, we first let the particles quickly scan the P-V curve and explore the possible peaks, and then slowly approach the optimal solution by a small-step perturbation. The velocity after the modification is given by:

$$\begin{aligned} v_i^{k+1} &= wv_i^k + c_1 r_1 (p_i - x_i^k) + c_2 r_2 (p_g - x_i^k) \ , v < |v_{\max}| \\ &\Rightarrow v_i^{k+1} = wv_i^k + (p_i + p_g - 2x_i^k) \end{aligned} \tag{24}$$

The transformation of this search pattern has the following benefits.

(1) Because there is no interference from the random variables, the trajectory of particle swarm optimization tends to be consistent, so the divergence of trajectories is avoided, and the global maximum can be quickly located by a small number of particles, which further reduces the computation cost.

(2) Compared with the standard PSO algorithm, the control structure is simplified. Among the control variables, except for the inertia weight which needs to be adjusted, the other parameters are displayed in a quantitative form, which makes the searching process more effective and controllable. By adjusting the inertia weight, the speed of power optimization of a photovoltaic array can be controlled effectively.

V. POWER TRACKING BY IPSO ALGORITHM

In the IPSO algorithm, the two-step method which combines the global searching model with the local searching model is adopted for tracking control. The algorithm flowchart is shown in Fig. 7.

Under the common circumstances, the solar radiation changes slowly. For instance, when the solar radiation fluctuates slightly or the photovoltaic panel is not shaded, because the maximum power point is near the operating point, the IPSO algorithm only operates in the local searching mode. On the other hand, when the solar radiation experiences a great fluctuation, for instance, when there is a shadow on a photovoltaic array, the global searching mode is started. In that case, the algorithm firstly enters a fast convergence state and approaches some possible peaks with a large step. By roughly comparing the values of several power peaks, it determines which peak may be the global maximum.

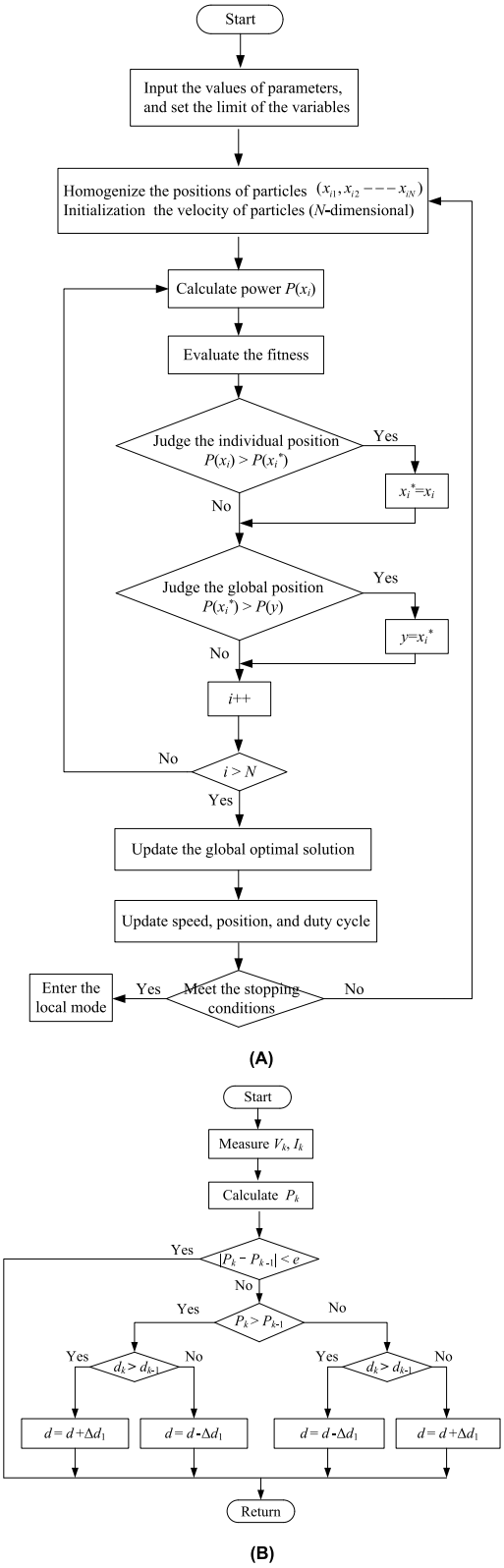

FIGURE 7. The algorithm flowchart; (A) Global search mode; (B) Local search mode.

Once the approximate position of the maximum power point is determined, the IPSO algorithm automatically switches to the local searching mode. Since the local searching mode

adopts the hill climbing method with a small disturbance, it is beneficial to get the exact position of power maximum.

A. STARTING CONDITIONS

Before the algorithm is started, the duty vector $\boldsymbol{d_g}$ that drives N particles is defined as:

$$d_g = [d_1, d_2, d_3, \ldots, d_N] \tag{25}$$

Also, the objective function of the optimized model is defined as:

$$f(x_i^k) > f(p_i) \tag{26}$$

where x_i^k is the location of the i^{th} particle in the k^{th} generation, and p_i is the best position that the i^{th} particle has experienced in the solution space.

If the speed vector is initialized to 0, the minimum value d_{min} and the maximum value $d_{\max}$ of the duty ratio are respectively calculated by:

$$d_{\min} = \frac{(\eta R_{L\min})^{\frac{1}{2}}}{(R_{PV\max})^{\frac{1}{2}} + (\eta R_{L\min})^{\frac{1}{2}}} \tag{27}$$

$$d_{\max} = \frac{(\eta R_{L\max})^{\frac{1}{2}}}{(R_{PV\min})^{\frac{1}{2}} + (\eta R_{L\max})^{\frac{1}{2}}} \tag{28}$$

where η is the converter efficiency, R_{Lmax} and R_{Lmin} are the maximum and minimum values of the output load, respectively, and R_{PVmax} and R_{PVmin} are the maximum and minimum impedances of a PV array, respectively.

As the photovoltaic array is laid outside, there are many factors that can affect the power output, such as natural fluctuation of solar radiation intensity, the passing of clouds over the sun, and tree shade. In order to discriminate among these influencing factors and reduce the unnecessary start of the algorithm, the automatic judgment on starting condition is needed, and the criterion is given by:

$$\left| \frac{I_{(x_i^{k+1})} - I_{(x_i^k)}}{I_{(x_i^k)}} \right| \geq \varepsilon_1 \tag{29}$$

$$\left| \frac{V_{(x_i^{k+1})} - V_{(x_i^k)}}{V_{(x_i^k)}} \right| \geq \varepsilon_2 \tag{30}$$

where $I(x_i^k)$ is the current value of the i^{th} particle in the k^{th} generation, $V(x_i^k)$ is the voltage value of the i^{th} particle in the k^{th} generation, $I(x_i^{k+1})$ is the current value of the i^{th} particle in the $(k+1)^{\text{th}}$ generation, $V(x_i^{k+1})$ is the voltage value of the i^{th} particle in the $(k+1)^{\text{th}}$ generation, and lastly ε_1 and ε_2 are the startup numbers, and generally, $\varepsilon_1 = 0.1, \varepsilon_2 = 0.2$. However, when the partial shadow is occluded, the single peak of the P-V curve transforms into multiple peaks. At the same time, the searching particles are also dispersed naturally to each peak of the P-V curve, which causes the power tracking to falls into a local optimum. If the voltage and current between the particles are quite different, namely, the conditions given by (29) and (30) are satisfied, and the shadow occlusion state of a PV array is confirmed, then the algorithm applies the global searching mode directly.

B. PARAMETER ADJUSTMENT

After simplifying the standard PSO algorithm, only one parameter, namely, the inertia weight needs to be adjusted. The adjustment steps are as follows.

(1) In the initial stage of algorithm operation, the inertia weight is set to be larger, which prevent the particle easily fall into a local optimum.

(2) In the later stage of algorithm operation, most of the particles are concentrated near the peaks. In that case, a smaller inertia weight is needed to make the convergence process stable.

Therefore, the strategy of the linearly decreasing weight (LDW) is added into the improved algorithm, specifically, by increasing the number of iterations, the inertia weight decreases; the specific calculation is given by:

$$w^k = \frac{k_{\max} - k}{k_{\max}}(w_{\max} - w_{\min}) + w_{\min} \tag{31}$$

where $w_{\max}$ represents the maximum inertia weight, $w_{\min}$ represents the minimum inertia weight, k is the number of current iteration, and $k_{\max}$ is the maximum number of iterations. In this study, w satisfies the following:

$$w^k = 0.9 - \frac{k}{k_{\max}} \times 0.5. \tag{32}$$

The value of the inertia weight is linearly decreasing from 0.9 to 0.4, which enables the algorithm to explore larger areas at the operation beginning to search for the global mode, and locate the approximate location of the optimal solution as fast as possible. As the number of iterations increases, the inertia weight becomes smaller. Then, the algorithm enters the local searching mode; thus, the searching range of the particle decreases, which is conducive to finding the maximum power point accurately.

C. TERMINATION STRATEGY

Since the algorithm performs an iterative search, the number of iterations should not be large. The iterative process stimulates power oscillation, which reduces the output power of a photovoltaic array. In order to avoid the endless searching for the maximum power point, a mandatory termination strategy is adopted in the proposed algorithm. According to the characteristics of the searching particles, they are initially distributed in the different locations on the P-V curve. As the search process proceeds, each particle will slowly gather around a certain peak. When the maximum voltage difference between the particles is no more than 5% of V_{oc}, the iteration terminates, and the algorithm stops.

In order to test the convergence of the proposed algorithm, we used the benchmark function of Griewank. There is a great interaction among the variables of the function, which has strong oscillation and many local points. It can be seen from Fig. 8. that compared with the standard PSO, the IPSO improves the convergence speed and search accuracy for the benchmark function.

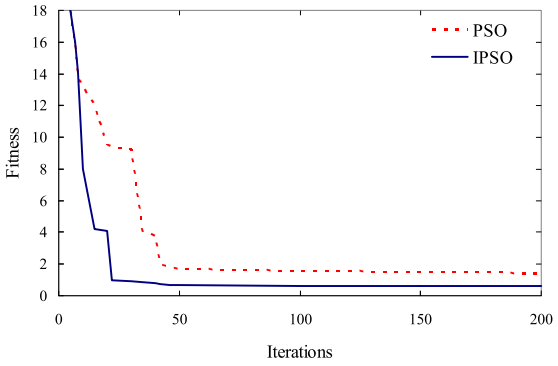

FIGURE 8. The fitness of Griewank function with the number of iterations.

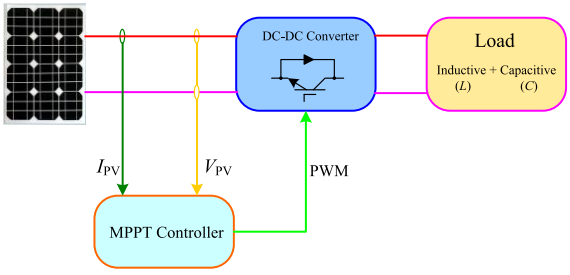

FIGURE 9. The block diagram of the PV system including the proposed MPPT.

VI. SIMULATION ANALYSIS

A. SIMULATION MODEL

The block diagram of a PV system under the partial shadowing, used in the simulation, is shown in Fig. 9. The duty ratio of the switching power supply was adjusted by the MPPT algorithm. When the input impedance of the DC-DC converter was changed, the equivalent load of the photovoltaic array also changed; the output voltage changed the final adjustment of the PV array so as to achieve maximum power point tracking. Finally, the maximum power point tracking was achieved by adjusting the output voltage of the photovoltaic array.

The simulation model was built by Matlab software, and the photovoltaic cell was modeled by BP Solar's Solarex-MSX60. The parameters in the handbook were as follows. The external reference temperature was 25 °C, and the external reference irradiance was 1000 W/m^2. The electrical parameters were: $P_{\max} = 60$ W, $V_{\mathrm{mp}} = 17.1$ V, $I_{\mathrm{mp}} = 3.5$ A, $I_{\mathrm{sc}} = 3.8$ A, and $V_{\mathrm{oc}} = 21.1$ V. The parameters of buck-boost circuit were: $C = 200$ uF, $L = 1.2$ mH, $f = 60$ KHz.

B. SIMULATION RESULTS

First, the simulation was run to obtain the *P-V* characteristic under the partial shading condition. The *P-V* characteristic curve is illustrated in Fig. 10. In Fig. 10, it can be observed that under the partial shading condition, the global MPP was at 140 V, and the corresponding output power was 2,720 W. In addition, one local MPP was found at 91 V and 2,503 W, and the other local MPP was at 170 V and 1860 W.

Next, we analyzed the dynamic behaviors by using the PSO and IPSO algorithms. The obtained dynamic response is

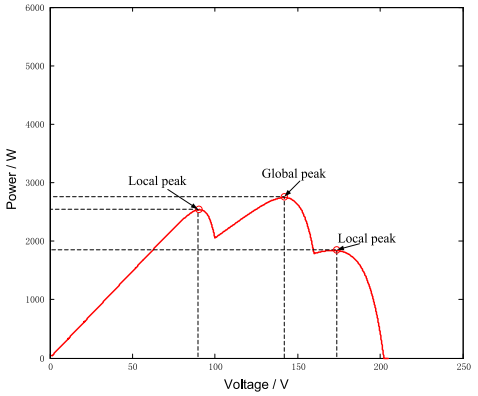

FIGURE 10. The P-V characteristic under the partial shadow.

illustrated in Fig. 11. In Figs. 11(A), (B), the power tracking effects of the standard PSO algorithm and the IPSO algorithm under the partial shading conditions at the number of particles $N_p = 4$ are presented. On the other hand, Figs. 11(C), (D) show the power tracking effects of the standard PSO algorithm and the IPSO algorithm under the partial shading conditions at the number of particles $N_p = 30$.

In Fig. 11, it can be seen that when the number of particles was $N_p = 4$, by using the standard PSO algorithm, the output power converged after 40 iterations, and the IPSO algorithm took only 22 iterations to achieve the convergence state. In addition, before reaching the convergence state, the standard PSO algorithm was accompanied by a large number of searching oscillations, so much energy was wasted. One reason for such a situation was that the standard PSO algorithm firstly searched between the local peaks and the global peak, so the convergence performance and the search speed depended on the acceleration factors and inertia weight. However, the IPSO algorithm firstly scanned the whole *P-V* curve, and then the searching particles were placed near the possible peak point, so the number of oscillations was reduced, which significantly increased the searching efficiency.

On the other hand, as the number of particles involved in the search increased, the number of searching iterations also increased, and the accuracy of power tracking was improved. When the number of particles was $N_p = 30$, the standard PSO algorithm needed 430 iterations to converge, while the IPSO algorithm took only 220 iterations to achieve convergence state; thus, the search efficiency was improved significantly.

Besides, the more particles were involved in the search, the more accurate the power tracking was. At $N_p = 4$, the maximum power that the particles could find was 2742 W, and the real maximum power was 2750 W. The difference between these two power values was 8 W, so the relative error was 0.3%. At $N_p = 30$, the maximum power that the particles could find was 2746 W, and the real maximum power point was 2750 W, so the difference between these two power values was 4 W, and the relative error was 0.15%.

Accordingly, the proposed IPSO algorithm had better convergence performance, it could find the maximum power point more accurately and quickly. Based on the simulation

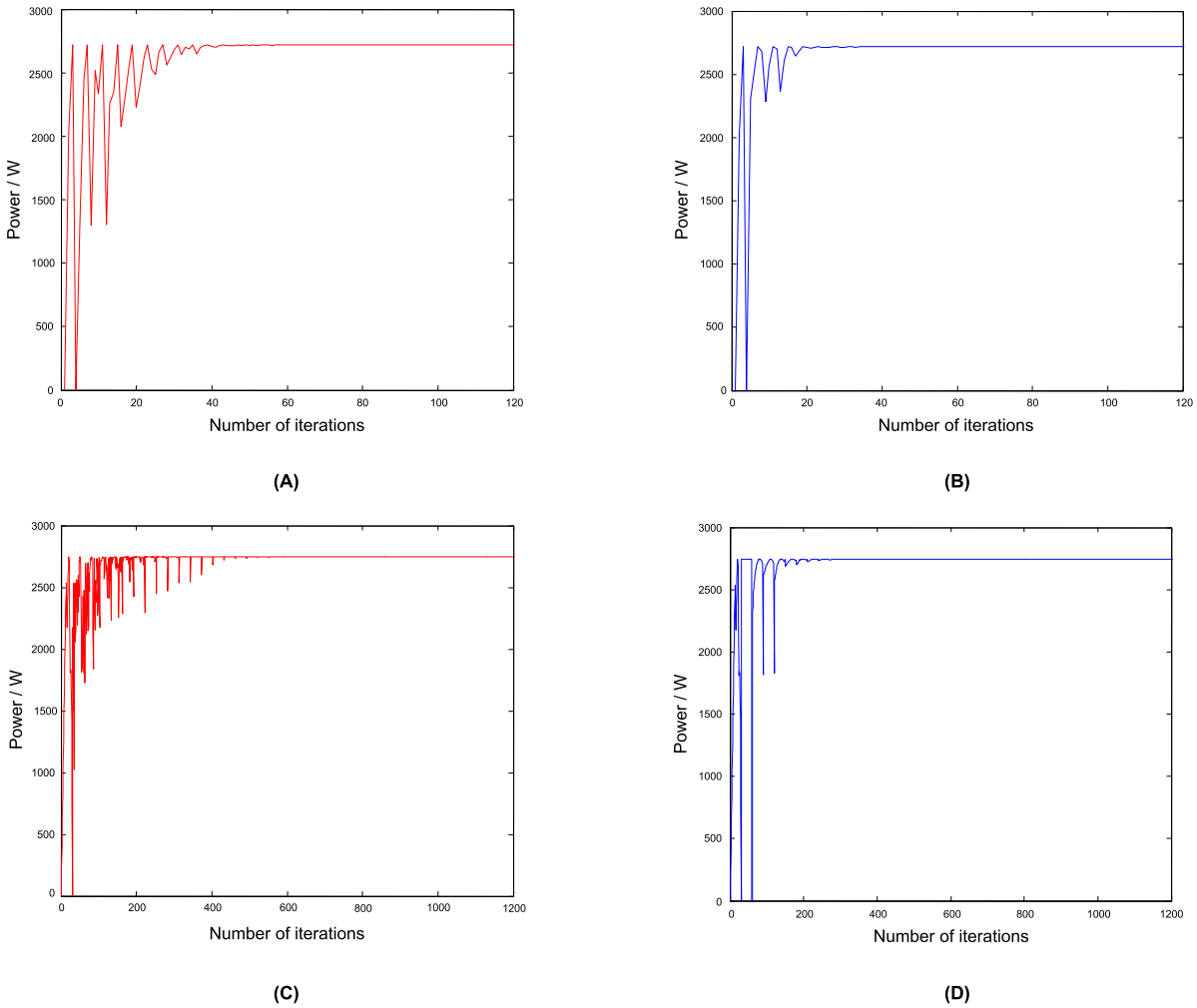

FIGURE 11. Comparison of simulation results obtained by the PSO and IPSO algorithms; (A) Power tracking used by standard PSO, $Np = 4$; (B) Power tracking used by IPSO, $Np = 4$; (C) Power tracking used by standard PSO, $Np = 30$; (D) Power tracking used by IPSO, $Np = 30$.

results, the accuracy of power tracking was improved with the increase in the number of searching particles at the cost of slower convergence speed and a large amount of calculation. Thus, the photovoltaic power tracking should be considered comprehensively in the specific application.

VII. EXPERIMENT

In order to evaluate the feasibility and stability of the proposed algorithm, the experimental system for the photovoltaic power tracking was designed. The experimental system composed of software and hardware. The hardware contained a photovoltaic module, the control circuit of power tracking, a personal computer, a DSP2812, and shielding material. The software environment included CCS3.3 and power monitoring program written in VC++. The communication between the hardware and software was realized through the serial port RS232. The experimental system is shown in Fig. 12(A).

The control circuit of photovoltaic power tracking was composed of the Boost power circuit, voltage and current detection circuit, signal sampling circuit, driving circuit of power transistors, as shown in Fig. 12(B).

Because the photovoltaic module had similar electrical characteristics as the photovoltaic array, the PV module was used in the experiment, and the partial area of the PV module was manually blocked. In this way, the *P-V* curve of the PV module might show the characteristics of multiple peaks. The control process was conducted by using DSP2812 and MPPT tracking circuits. Using the human-computer interaction interface written in Visual C++ and the SQL database, the scanned data were stored and displayed, as shown in Fig.13.

The photovoltaic module parameters were listed at Table 1. During the experiment, the same irradiation and temperature variation were used for all the methods.

The steady-state performance of the photovoltaic module for patterns 1, 2, and 3 is shown in Fig. 13. Pattern 1 referred to the shading at shelter #1 position, at this moment there were one GMPP and one LMPP, and the power at GMPP was 53.8W. Pattern 2 referred to the shading at shelter #2 position,

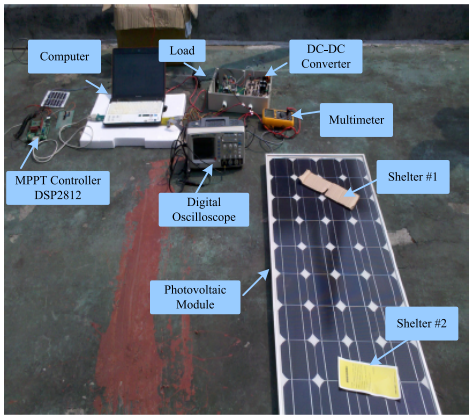

(A)

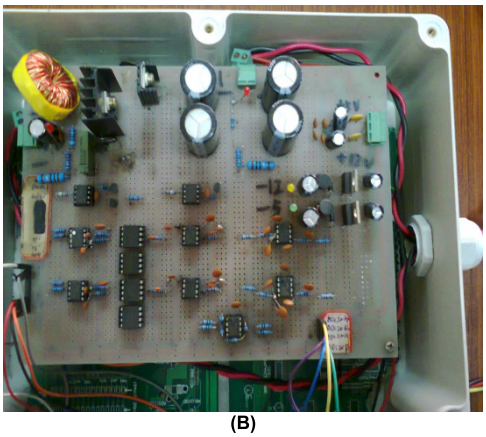

(B)

FIGURE 12. Experimental platform; (A) The experimental system for photovoltaic power tracking; (B) The control circuit of photovoltaic power tracking.

TABLE 1. Parameter of PV module at Temperature = 25 °C, Irradiation = 1000 W/m^2.

Maximum Power (P_{max})	80W
Voltage at MPP (V_{mpp})	19.8V
Current at MPP (I_{mpp})	4.04A
Open Circuit Voltage (V_{oc})	24V
Short Circuit Current (I_{sc})	4.29A

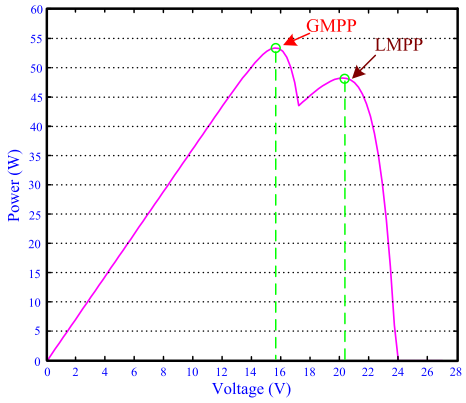

(A)

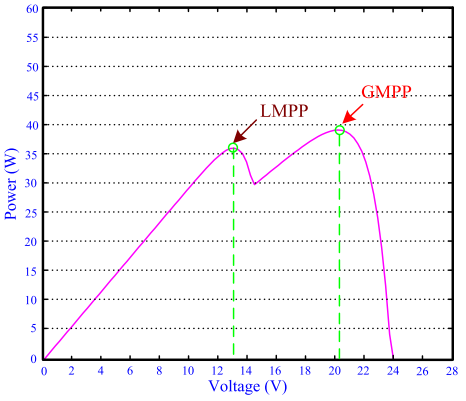

(B)

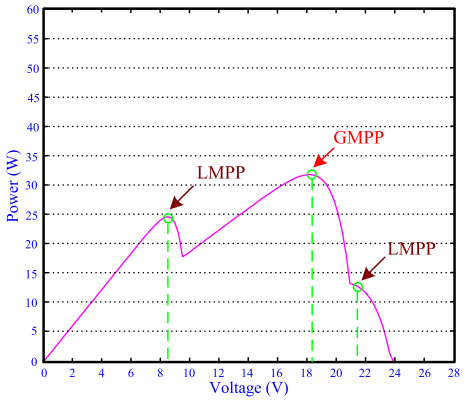

(C)

FIGURE 13. The *P-V* characteristic at different positions occluded on the photovoltaic module; (A) *P-V* characteristic curve, shelter #1 position; (B) *P-V* characteristic curve, shelter #2 position; (C) *P-V* characteristic curve, shelter #1 and #2 positions at the same time.

at this moment there were one GMPP and one LMPP, and the power at GMPP was 38.7W. Pattern 3 referred to the shading at both shelter #1 and #2 positions at the same time, there were one GMPP and two LMPPs, and the power at GMPP was 32.6W.

The waveforms of voltage, current, and power, which were obtained by the PSO, the IPSO, and the FLC algorithms under the dynamic condition are shown in Fig. 14. For each waveform, the tracking time (T_{MPPT}) and algorithm were mentioned manually. The GMPP tracking time of all the algorithms on all the patterns is given in Table 2.

For comparison, the experimental results for conventional PSO was obtained for partially shaded pattern 1, 2 and 3 as shown in Fig. 14. The conventional PSO took 3.4 s, 3.6 s and 3.9 s to reach the GMPP in three patterns respectively. Because PSO algorithm is affected by random variables, it can not converge in a fixed direction at first, so it takes a long time to locate GMPP accurately. The conventional FLC took 3.8 s, 3.9 s and 4.1 s to reach the GMPP in three patterns respectively. Although the conventional FLC reduces the disturbance of variables, it is essentially a non-linear control, the searching time for maximum power point is longer. The IPSO took 2.9 s, 3.0 s and 3.2 s to reach the GMPP in three patterns respectively. The IPSO uses global localization

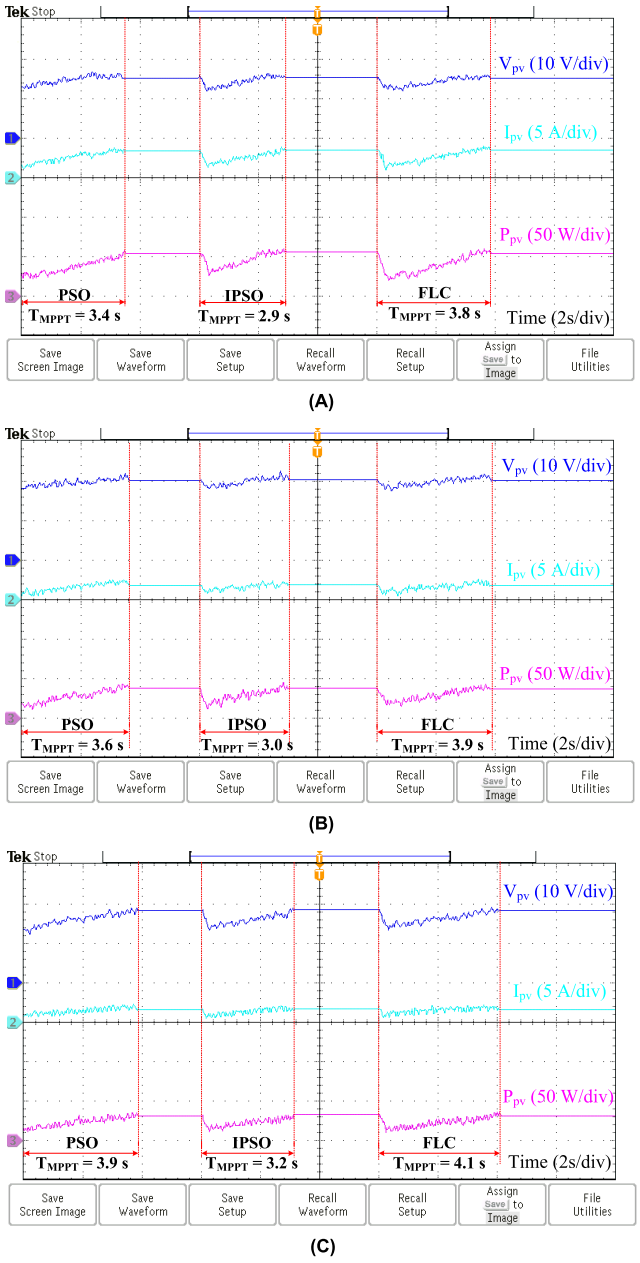

FIGURE 14. Experimental results of the PSO, the IPSO, and the FLC algorithms; (A) Experimental results of the PSO, the IPSO, and the FLC algorithms in the case of pattern 1; (B) Experimental results of the PSO, the IPSO, and the FLC algorithms in the case of pattern 2; (C) Experimental results of the PSO, the IPSO, and the FLC algorithms in the case of pattern 3.

and local convergence, so the convergence speed is obviously better than PSO and FLC.

In Fig. 14, the time division on the x-axis was 2 s/div, and on every 6 s the algorithm was changed another. The experimental results are summarized in Table 2 and Table 3. Table 2 reveals that the IPSO reached the GMPP at every pattern in only 3.0 s on average, while the PSO and FLC took 3.6 s and 3.9 s for the same task. Table 3 shows that the tracking accuracy of IPSO was more than 99% in three shading patterns. Since IPSO firstly differentiates the power

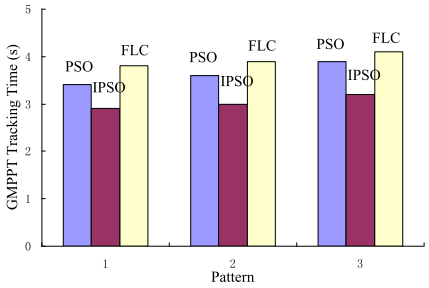

FIGURE 15. Performance comparison of the MPPT algorithms in the experiment.

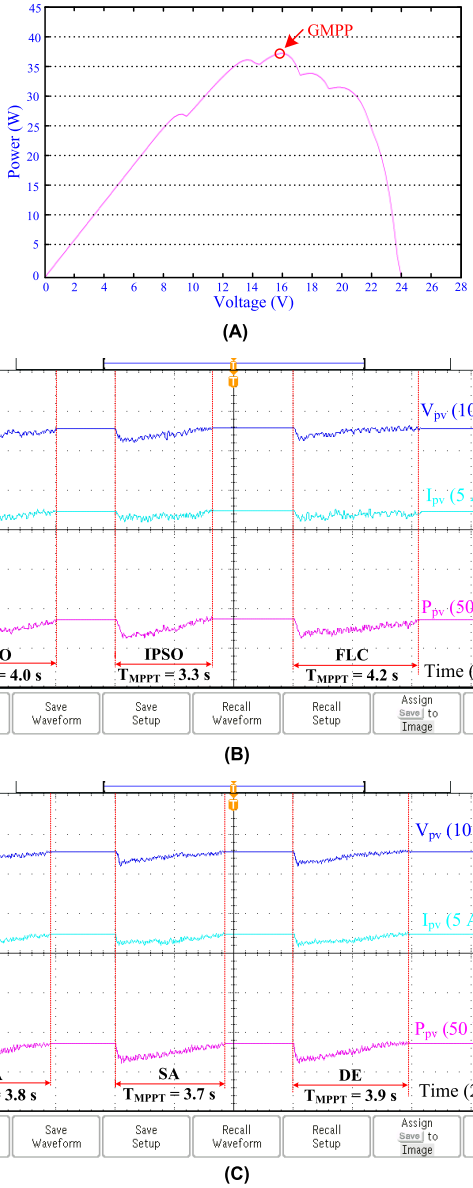

FIGURE 16. Experimental results including multiple power points; (A) *P-V* characteristic curve; (B) Experimental results of the PSO, the IPSO, and the FLC algorithms with multiple power points; (C) Experimental results of the GA, the SA and the DE with multiple power points.

points, then it immediately turns to the local searching mode, which is conducive to the accurate location of the maximum power point.

TABLE 2. Tracking time for patterns 1, 2 and 3.

Pattern	PSO Tracking Time (s)	IPSO Tracking Time (s)	FLC Tracking Time (s)
1	3.4	2.9	3.8
2	3.6	3.0	3.9
3	3.9	3.2	4.1

TABLE 3. Tracking accuracy for patterns 1, 2 and 3.

Pattern	PSO Tracking accuracy (%)	IPSO Tracking accuracy (%)	FLC Tracking accuracy (%)
1	98.9	99.4	98.8
2	98.6	99.3	98.5
3	98.5	99.3	98.4

The obtained voltage, current, and power waveforms are given in Fig. 14. In Fig. 14, the searching area, as well as the oscillations in the output waveform during the searching process can be observed. Since the duration of major oscillations was directly proportional to the tracking time, the major oscillations in the PSO algorithm were approximately 11.3% longer than that of the IPSO algorithm. Similarly, the oscillations of the FLC algorithm were approximately 12.2% longer than that of the IPSO algorithm.

The comparison of the algorithms regarding the tracking performance for all the patterns in the experiment is presented by the bar-chart in Fig. 15, where it can be seen that the performance of the IPSO was the best on all the patterns. The average tracking time of the PSO, the IPSO, and the FLC in the experiment was 3.6 s, 3.0 s, and 3.9 s, respectively.

In order to verify the effectiveness of the proposed algorithm, we carried out the tracking experiment including five power points, as shown in Fig. 16. It can be seen that the IPSO kept good tracking performance as before. It not only had fast tracking speed, but also could lock the maximum power point in only 3.3 s, and the tracking accuracy also reached 99%. Compared with five recently developed Global MPPT algorithms, the proposed IPSO shows better tracking performance.

VIII. CONCLUSION

This paper introduces an improved power tracking algorithm for a photovoltaic array under a local shadow. Based on the analysis of the particle swarm optimization (PSO) algorithm and the electrical characteristics of the photovoltaic arrays, an improved particle swarm optimization (IPSO) is proposed for the MPP detection under the PSC. The main contributions of this work are as follows.

(1) The traditional PSO algorithm is profoundly studied. Aiming at the convergence problem of the PSO algorithm and the influence of random variables on the particle trajectory, the convergence conditions of the PSO algorithm are analyzed, which provides a theoretical basis for improving the PSO algorithm.

(2) The traditional PSO algorithm is improved, and the concrete realization principle of the IPSO algorithm is introduced. Due to the combining of global and local searching modes, the proposed algorithm is especially suitable for the power tracking of a photovoltaic array under local shadows.

(3) The experiment of the GMPPT of the photovoltaic module is conducted under the local shading conditions. The experimental results show that under the same conditions, compared with five recently developed Global MPPT algorithms, the performance of the IPSO in the GMPPT under the PSC is improved significantly.

APPENDIX

When the experimental system works, the output voltage V_{pv}, current I_{pv} of the photovoltaic module and input voltage V_{load} and current I_{load} of the load are sampled continuously by DSP2812. The output power P_{pv} and load power consumption P_{load} can be calculated in real time.

Experimental diagram.

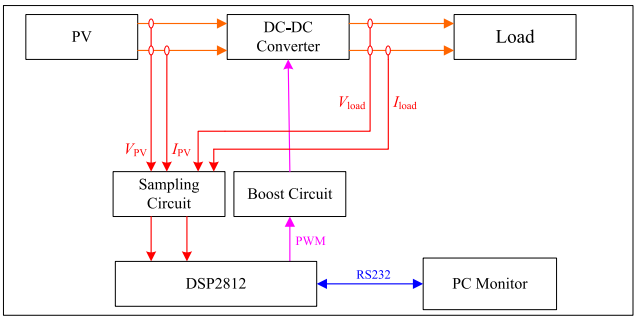

FIGURE 17. Experimental diagram.

REFERENCES

[1] M. Abdel-Salam, M.-T. El-Mohandes, and M. Goda, "An improved perturb-and-observe based MPPT method for PV systems under varying irradiation levels," *Solar Energy*, vol. 171, pp. 547–561, Sep. 2018.

[2] J. Ahmed and Z. Salam, "An enhanced adaptive P&O MPPT for fast and efficient tracking under varying environmental conditions," *IEEE Trans. Sustain. Energy*, vol. 9, no. 3, pp. 1487–1496, Jul. 2018.

[3] V. R. Kota and M. N. Bhukya, "A novel linear tangents based P&O scheme for MPPT of a PV system," *Renew. Sustain. Energy Rev.*, vol. 71, pp. 257–267, May 2017.

[4] S. S. Mohammed, D. Devaraj, and T. P. I. Ahamed, "A novel hybrid maximum power point tracking technique using perturb & observe algorithm and learning automata for solar PV system," *Energy*, vol. 112, pp. 1096–1106, Oct. 2016.

[5] S. Necaibia, M. SamiraKelaiaia, H. Labar, A. Necaibia, and E. D. Castronuovo, "Enhanced auto-scaling incremental conductance MPPT method, implemented on low-cost microcontroller and SEPIC converter," *Solar Energy*, vol. 180, pp. 152–168, Mar. 2019.

[6] E. Kandemir, S. Borekci, and N. S. Cetin, "Comparative analysis of reduced-rule compressed fuzzy logic control and incremental conductance MPPT methods," *J. Electron. Mater.*, vol. 47, no. 8, pp. 4463–4474, Aug. 2018.

[7] A. Amir, A. Amir, J. Selvaraj, N. A. Rahim, and A. M. Abusorrah, "Conventional and modified MPPT techniques with direct control and dual scaled adaptive step-size," *Solar Energy*, vol. 157, pp. 1017–1031, Nov. 2017.

[8] N. E. Zakzouk, M. A. Elsaharty, A. K. Abdelsalam, A. A. Helal, and B. W. Williams, "Improved performance low-cost incremental conductance PV MPPT technique," *IET Renew. Power Gener.*, vol. 10, no. 4, pp. 561–574, Apr. 2016.

[9] H. Renaudineau, F. Donatantonio, J. Fontchastagner, G. Petrone, G. Spagnuolo, J.-P. Martin, and S. Pierfederici, "A PSO-based global MPPT technique for distributed PV power generation," *IEEE Trans. Ind. Electron.*, vol. 62, no. 2, pp. 1047–1058, Feb. 2015.

[10] K. S. Tey and S. Mekhilef, "Modified incremental conductance algorithm for photovoltaic system under partial shading conditions and load variation," *IEEE Trans. Ind. Electron.*, vol. 61, no. 10, pp. 5384–5392, Oct. 2014.

[11] Q. Zhu, X. Zhang, S. Li, C. Liu, and H. Ni, "Research and test of power-loop-based dynamic multi-peak MPPT algorithm," *IEEE Trans. Ind. Electron.*, vol. 63, no. 12, pp. 7349–7359, Dec. 2016.

[12] J. Ahmed and Z. Salam, "An accurate method for MPPT to detect the partial shading occurrence in a PV System," *IEEE Trans. Ind. Informat.*, vol. 13, no. 5, pp. 2151–2161, Oct. 2017.

[13] T. Radjai, J. P. Gaubert, L. Rahmani, and S. Mekhilef, "Experimental verification of P&O MPPT algorithm with direct control based on Fuzzy logic control using CUK converter," *Int. Trans. Electr. Energy Syst.*, vol. 25, no. 12, pp. 3492–3508, Dec. 2015.

[14] T. Radjai, L. Rahmani, S. Mekhilef, and J. P. Gaubert, "Implementation of a modified incremental conductance MPPT algorithm with direct control based on a fuzzy duty cycle change estimator using dSPACE," *Sol. Energy*, vol. 110, pp. 325–337, Dec. 2014.

[15] S. Messalti, A. Harrag, and A. Loukriz, "A new variable step size neural networks MPPT controller: Review, simulation and hardware implementation," *Renew. Sustain. Energy Rev.*, vol. 68, Part 1, pp. 221–233, Feb. 2017.

[16] S. Mohanty, B. Subudhi, and P. K. Ray, "A grey wolf-assisted perturb & observe MPPT algorithm for a PV system," *IEEE Trans. Energy Convers.*, vol. 32, no. 1, pp. 340–347, Mar. 2017.

[17] R. Tang, Z. Wu, and Y. Fang, "Configuration of marine photovoltaic system and its MPPT using model predictive control," *Solar Energy*, vol. 158, pp. 995–1005, Dec. 2017.

[18] S. Moon, S.-G. Yoon, and J.-H. Park, "A new low-cost centralized MPPT controller system for multiply distributed photovoltaic power conditioning modules," *IEEE Trans. Smart Grid*, vol. 6, no. 6, pp. 2649–2658, Nov. 2017.

[19] R. L. Tang, Z. Wu, and Y. J. Fang, "Topological structure of large-scale photovoltaic array and its MPPT controlling method," *Energy Procedia*, vol. 105, pp. 113–118, May 2017.

[20] S. Lyden and M. E. Haque, "A simulated annealing global maximum power point tracking approach for PV modules under partial shading conditions," *IEEE Trans. Power Electron.*, vol. 31, no. 6, pp. 4171–4181, Jun. 2016.

[21] P. Lei, Y. Li, and J. E. Seem, "Sequential ESC-based global MPPT control for photovoltaic array with variable shading," *IEEE Trans. Sustain. Energy*, vol. 2, no. 3, pp. 348–358, Jul. 2011.

[22] N. Bizon, "Global extremum seeking control of the power generated by a photovoltaic array under partially shaded conditions," *Energy Convers. Manage.*, vol. 109, pp. 71–85, Feb. 2016.

[23] R. Sridhar, S. Jeevananthan, S. S. Dash, and P. Vishnuram, "A new maximum power tracking in PV system during partially shaded conditions based on shuffled frog leap algorithm," *J. Exp. Theor. Artif. Intell.*, vol. 29, no. 3, pp. 481–493, 2016.

[24] B.-R. Peng, K.-C. Ho, and Y.-H. Liu, "A novel and fast MPPT method suitable for both fast changing and partially shaded conditions," *IEEE Trans. Ind. Electron.*, vol. 65, no. 4, pp. 3240–3251, Apr. 2018.

[25] N. Kumar, I. Hussain, B. Singh, and B. K. Panigrahi, "Rapid MPPT for uniformly and partial shaded PV system by using JayaDE algorithm in highly fluctuating atmospheric conditions," *IEEE Trans. Ind. Informat.*, vol. 13, no. 5, pp. 2406–2416, Oct. 2017.

[26] K. L. Lian, J. H. Jhang, and I. S. Tian, "A maximum power point tracking method based on perturb-and-observe combined with particle swarm optimization," *IEEE J. Photovolt.*, vol. 4, no. 2, pp. 626–633, Mar. 2014.

[27] H. Fathabadi, "Novel fast dynamic MPPT (maximum power point tracking) technique with the capability of very high accurate power tracking," *Energy*, vol. 94, pp. 466–475, Jan. 2016.

[28] H. Abouadane, A. Fakkar, Y. Elkouari, and D. Ouoba, "Performance of a new MPPT method for Photovoltaic systems under dynamic solar irradiation profile," *Energy Procedia*, vol. 142, pp. 538–544, Dec. 2017.

[29] D. Ouoba, A. Fakkar, Y. E. Kouari, F. Dkhichi, and B. Oukarfi, "An improved maximum power point tracking method for a photovoltaic system," *Opt. Mater.*, vol. 56, pp. 100–106, Jun. 2016.

[30] K. S. Tey, S. Mekhilef, M. Seyedmahmoudian, B. Horan, A. T. Oo, and A. Stojcevski, "Improved differential evolution-based MPPT algorithm using SEPIC for PV systems under partial shading conditions and load variation," *IEEE Trans. Ind. Informat.*, vol. 14, no. 10, pp. 4322–4333, Oct. 2018.

[31] T. K. Soon and S. Mekhilef, "A fast-converging MPPT technique for photovoltaic system under fast-varying solar irradiation and load resistance," *IEEE Trans Ind. Informat.*, vol. 11, no. 1, pp. 176–186, Feb. 2015.

[32] M. Seyedmahmoudian, B. Horan, T. K. Soon, R. Rahmani, A. M. T. Oo, S. Mekhilef, and A. Stojcevski, "State of the art artificial intelligence-based MPPT techniques for mitigating partial shading effects on PV systems—A review," *Renew. Sustain. Energy Rev.*, vol. 64, pp. 435–455, Oct. 2016.

[33] R. B. A. Koad and A. F. Zobaa, "Comparison between the conventional methods and PSO based MPPT algorithm for photovoltaic systems," *Int. J. Elect., Robot., Electron. Commun. Eng.*, vol. 8, no. 4, pp. 673–678, 2014.

[34] F. M. D. Oliveira, S. A. O. da Silva, F. R. Durand, L. P. Sampaio, V. D. Bacon, and L. B. G. Campanhol, "Grid-tied photovoltaic system based on PSO MPPT technique with active power line conditioning," *IET Power Electron.*, vol. 9, no. 6, pp. 1180–1191, May 2016.

[35] O. B. Belghith, L. Sbita, and F. Bettaher, "MPPT design using PSO technique for photovoltaic system control comparing to fuzzy logic and P&O controllers," *Energy Power Eng.*, vol. 8, no. 11, 2016, Art. no. 72396.

[36] J. Shi, W. Zhang, Y. Zhang, F. Xue, and T Yang, "MPPT for PV systems based on a dormant PSO algorithm," *Electric Power Syst. Res.*, vol. 123, pp. 100–107, Jun. 2015.

[37] S. M. Mirhassani, S. Z. M. Golroodbari, S. M. M. Golroodbari, and S. Mekhilef, "An improved particle swarm optimization based maximum power point tracking strategy with variable sampling time," *Int. J. Elect. Power Energy Syst.*, vol. 64, pp. 761–770, Jan. 2015.

[38] S. Rajendran and H. Srinivasan, "Simplified accelerated particle swarm optimisation algorithm for efficient maximum power point tracking in partially shaded photovoltaic systems," *IET Renew. Power Gener.*, vol. 10, no. 9, pp. 1340–1347, Oct. 2016.

[39] N. Bouarroudj, D. Boukhetala, A. Djari, Y. Rais, and B. Benlahbib, "FLC based Gaussian membership functions tuned by PSO and GA for MPPT of photovoltaic system: A comparative study," in *Proc. 6th Int. Conf. Syst. Control (ICSC)*, May 2017, pp. 317–322.

[40] K. Kaced, C. Larbes, S. M. Ait-Chikh, M. Bounabi, and Z. E. Dahmane, "FPGA implementation of PSO based MPPT for PV systems under partial shading conditions," in *Proc. 6th Int. Conf. Syst. Control (ICSC)*, May 2017, pp. 150–155.

[41] R. Subha and S. Himavathi, "A performance comparison of PSO based MPPT algorithms for various partial shading conditions," *Indian J. Sci. Technol.*, vol. 9, no. 45, pp. 1–7, Dec. 2016.

[42] M. Abdulkadir, A. L. Bukar, and B. Modu, "MPPT-based control algorithm for PV system using iteration-PSO under irregular shadow conditions," *Arid Zone J. Eng., Technol. Environ.*, vol. 13, no. 1, pp. 97–110, Feb. 2017.

[43] D. M. Sullivan, "Z-transform theory and the FDTD method," *IEEE Trans. Antennas Propag.*, vol. 44, no. 1, pp. 28–34, Jan. 1996.

KEYONG HU received the Ph.D. degree in mechatronic engineering from the Zhejiang University of Technology, Hangzhou, China, in 2016. He is currently a Teacher of electronic information engineering with Qianjiang College, Hangzhou Normal University. His research interests include artificial intelligence and new energy technology.

SHIHUA CAO received the Ph.D. degree from the Macau University of Science and Technology. He was a Visiting Professor with the University of North Texas, Denton, TX, USA, from 2013 to 2014. He is currently a Professor and a Senior Engineer with Qianjiang College, Hangzhou Normal University. His research interests include wireless sensor networks, radio frequency energy harvesting, and vital signal monitoring smart health.

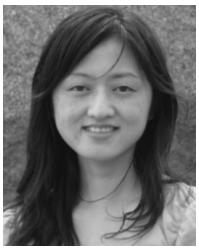

WENJUAN LI received the Ph.D. degree in computer science from Zhejiang University, Hangzhou, China, in 2012. She is currently an Associate Professor with Hangzhou Normal University and a Visiting Scholar with the CLOUDS Lab, The University of Melbourne. She holds a postdoctoral position with Shanghai Jiao Tong University. Her research interests include cloud computing, and social networks and trust.

FANGMING ZHU received the M.S. degree in radio engineering from Southeast University, China, in 1994, and the Ph.D. degree from Zhejiang University, in 2004. She served as a Teacher with the Department of Optoelectronic Information Engineering, Zhejiang University. She is currently an Associate Professor with Hangzhou Normal University. Her research interests include surface plasmon polaritons and advanced devices, Novel antenna on metamaterials, RFID antenna, RFID systems, and application of the Internet of Things.